

Impurity effect as a probe of the paring symmetry in BiS₂-based superconductors

S. L. Liu¹

¹*College of Science, Nanjing University of Posts and Telecommunications,
Nanjing 210003, China*

(Dated: November 12, 2018)

The impurity effects are studied for the BiS₂-layered superconductors based on a two-orbital model with the Bogoliubov-de-Gennes technique. The superconducting critical temperature (T_c) is calculated as a function of the impurity concentration. Significant reduction of T_c is found for the spin singlet nearest-neighboring paring d-wave state and the spin triplet next-nearest-neighboring (NNN) paring p-wave state, but no depression of T_c for isotropic s-wave state. The single impurity effects for various paring states are also explored. The impurity resonance peak in the local density of states spectrum is found only for the d-wave state. For the spin triplet NNN paring p-wave state, two in-gap peaks occur in the case of positive impurity potential and a single in-gap peak is found for the negative impurity potential, and it shifts towards the lower energy with the potential strength decreasing. These results can be used to detect the paring symmetry of the BiS₂-based superconductors.

PACS numbers: 74.70.Xa, 74.55.+v

Superconductors with layered crystal structures such as cuprates¹, Sr₂RuO₄², MgB₂³, Na_xCo₂O₂⁴ and iron pnictides⁵ have generated enormous research interest. The low dimensionality can affect the electronic structure and can realize high transition temperatures and/or unconventional superconductivity mechanisms. Quite recently, superconductivity has been observed in the BiS₂-based compounds⁶, such as Bi₄O₄S₃⁶, LaO_{1-x}F_xBiS₂⁷, NdO_{1-x}F_xBiS₂⁸, CeO_{1-x}F_xBiS₂⁹, and PrO_{0.5}F_{0.5}BiS₂¹⁰, where the BiS₂-layer is a basic unit. Soon after that, considerable efforts have been paid on the investigation of the physical properties in this system¹¹⁻²⁵. The discovery of the new basic superconducting (SC) layers may open new fields in physics and chemistry of low-dimensional superconductors.

The BiS₂-based materials compose of the stacking of BiS₂-SC layers and the spacer layers, which resembles those of high- T_c cuprates and the Fe-based superconductors. The first principle band structure calculations^{6,11} predict that the dominating bands for the electron conduction as well as for the superconductivity are derived from the Bi $6p_x$ and $6p_y$ orbits. According to the Hall effect and the magnetoresistance measurements¹², an exotic multi-band feature is found in the Bi₄O₄S₃ compounds and the SC pairing occurs in the one-dimensional chains. Electrical resistivity measurements under pressure¹⁶ reveal that Bi₄O₄S₃ and LaO_{1-x}F_xBiS₂ have different T_c versus pressure behavior, and the Fermi surface of LaO_{1-x}F_xBiS₂ may be located in the vicinity of some band edges, which leads to the instability for superconductivity. It is found that the parent phase is a bad metal in the CeO_{1-x}F_xBiS₂ system⁹, while a band insulator in the case of Bi₄O₄S₃ compounds⁶. By doping electrons into the system, superconductivity appears together with an insulating normal state⁹, which is obviously different from that of the cuprates and the iron pnictides.

The most fundamental issue in this BiS₂-based com-

pound is the superconductivity mechanism, which is still unclear. It is predicted that the electron-phonon coupling constant is as large as $\lambda = 0.85$, which indicates that LaO_{1-x}F_xBiS₂ is a strongly coupled electron-phonon superconductor^{18,19}. However, because electron-electron correlation generally is more important in a low dimensional system, the correlation effect might play an important role in driving superconductivity even if the p -orbits of Bi are much less localized compared with the d -orbits in cuprates and iron-based superconductors²⁶. Experimentally, no magnetically ordered phase has been detected so far in the BiS₂ compounds. This apparent absence of magnetism in the BiS₂ compounds may still locate them in the same category as LiFeAs, FeSe, and possibly Sr₂VO₃FeAs, which are also non magnetic but their pairing properties are widely believed to still be originated from the short-range magnetic fluctuations²⁷. Moreover, a good nesting of the Fermi surface at wave vector $\mathbf{k} = (\pi, \pi, 0)$ has been found^{11,18}. It is also proposed that the SC pairing is strong and it exceeds the limit of the phonon mediated picture¹². The anharmonic model calculation shows that the vicinity of the charge-density-wave instability is essential for the superconductivity¹⁸. It is reminiscent to the proximity to spin-density-wave of iron pnictides, which is well established⁵. The correlation effect, therefore, seems to be a good candidate responsible for the SC pairing in these materials. Thus, the spin fluctuation is also proposed to account for the SC pairing in this family^{17,26,27}.

Another puzzle is the SC paring symmetry of the BiS₂-based superconductors. Due to the large electron-phonon coupling constant, the paring symmetry may usually be a conventional s-wave state with isotropic SC gap. However, the correlation effect is also proposed to account for the SC paring, which may lead to the paring symmetry in a complicated situation in these compounds. Moreover, based on the the first principle calculation¹¹, it is found that the Fermi level for the nominal compo-

sition is located in the vicinity of the topological change in the Fermi surface. This gives a possibility that the SC symmetry changes depending on the doping level, provided that the superconductivity originates from the electric correlation. Considering various many-body interactions, possible pairing states are proposed, such as sign conserving/reversing s-wave and d-wave states^{11,17}. Furthermore, the first principle calculation indicates the quasi-one-dimensional bands¹¹, which may lead to the spin-triplet pairing. In the $\text{CeO}_{1-x}\text{F}_x\text{BiS}_2$ compounds, superconductivity and ferromagnetism (FM) are found to coexist⁹, where FM may arise from the Ce moments. The coexistence of superconductivity and FM challenges the spin-singlet pairing mechanism, which reminds us of the Sr_2RuO_4 material, whose short-range ferromagnetic spin fluctuations give rise to the triplet pairing with p-like symmetry²⁸.

The impurity effect is one of the most important tools for identifying the nature of the pairing state and the microscopic properties, which has been successfully carried out in both conventional superconductors²⁹ and unconventional ones, such as cuprates³⁰ and iron pnictides^{31–34,36,37,44}. In this paper, we will study theoretically the impurity effect in the BiS_2 -based materials and look into the pairing symmetry based on the two-orbital model¹¹ and the Bogoliubov-de-Gennes (BdG) equations. The impurity concentration dependence of the critical temperature is explored. Significant reduction of T_c is found for the spin singlet nearest-neighboring (NN) pairing d-wave state and the spin triplet next-nearest-neighboring (NNN) pairing p-wave state, while no depression of T_c for isotropic s-wave state. The single impurity effects for various pairing states are also calculated. The impurity resonance peak in the local density of states (LDOS) spectrum is found only for the d-wave state. The evolution of the resonance peak with the impurity strength is calculated as well. For the spin triplet NNN pairing p-wave state, two in-gap peaks occur in the case of positive impurity potential and a single in-gap peak is found for the negative impurity potential, and it shifts towards the lower energy with the decreasing of the potential strength. These results can be used to detect the pairing symmetry of the BiS_2 -based superconductors.

The starting model Hamiltonian with the hopping elements, the pairing terms and the impurity part is expressed by

$$H = H_t + H_\Delta + H_{\text{imp}}. \quad (1)$$

In the present work, we use the two-orbital model with the hopping constants from Ref. 11. Thus, the hopping term H_t can be expressed by

$$H_t = - \sum_{i\mu j\nu\sigma} (t_{i\mu j\nu} c_{i\mu\sigma}^\dagger c_{j\nu\sigma} + \text{H.c.}) - t_0 \sum_{i\mu\sigma} c_{i\mu\sigma}^\dagger c_{i\mu\sigma}, \quad (2)$$

where i, j are the site indices, $\mu, \nu = 1, 2$ are the orbital indices, and t_0 is the chemical potential. Considering the possibilities of both spin singlet and triplet pairings, the

pairing term is written as

$$H_\Delta = \sum_{ij} [\Delta_{i\mu j\nu}^\pm (c_{i\mu\uparrow}^\dagger c_{j\nu\downarrow}^\dagger \pm c_{i\mu\downarrow}^\dagger c_{j\nu\uparrow}^\dagger) + \text{H.c.}]. \quad (3)$$

Here, \pm is for spin-triplet and singlet pairings respectively, and the pairing potential $\Delta_{i\mu j\nu}^\pm$ is defined as $\Delta_{i\mu j\nu}^\pm = \frac{V_{i\mu j\nu}}{2} (\langle c_{i\mu\uparrow} c_{j\nu\downarrow} \rangle \pm \langle c_{i\mu\downarrow} c_{j\nu\uparrow} \rangle)$, where $V_{i\mu j\nu}$ is the SC interaction. H_{imp} is the impurity part of the Hamiltonian, written as

$$H_{\text{imp}} = \sum_{i_m\mu\sigma} V_s c_{i_m\mu\sigma}^\dagger c_{i_m\mu\sigma}. \quad (4)$$

In this paper, both single- and multiple- impurity effects are studied, and following Refs. 29, 30 and 36, only the intraorbital scattering by nonmagnetic impurities is considered.

Then, the Hamiltonian can be diagonalized by solving the BdG equations self-consistently,

$$\sum_j \sum_\nu \begin{pmatrix} H_{i\mu j\nu\sigma} & \Delta_{i\mu j\nu}^\pm \\ \mp \Delta_{i\mu j\nu}^{\pm*} & -H_{i\mu j\nu\bar{\sigma}}^* \end{pmatrix} \begin{pmatrix} u_{j\nu\sigma}^n \\ v_{j\nu\bar{\sigma}}^n \end{pmatrix} = E_n \begin{pmatrix} u_{i\mu\sigma}^n \\ v_{i\mu\bar{\sigma}}^n \end{pmatrix}, \quad (5)$$

where the Hamiltonian $H_{i\mu j\nu\sigma}$ is expressed by,

$$H_{i\mu j\nu\sigma} = -t_{i\mu j\nu} - t_0 \delta_{ij} \delta_{\mu\nu} + \sum_{i_m} V_s \delta_{i, i_m}. \quad (6)$$

The SC order parameter $\Delta_{i\mu j\nu}$ and the local electron density $\langle n_{i\mu} \rangle$ are obtained self-consistently:

$$\Delta_{i\mu j\nu}^\pm = \frac{V_{i\mu j\nu}}{4} \sum_n (u_{i\mu\uparrow}^n v_{j\nu\downarrow}^{n*} \mp u_{j\nu\uparrow}^n v_{i\mu\downarrow}^{n*}) \tanh\left(\frac{E_n}{2k_B T}\right), \quad (7)$$

$$\langle n_{i\mu} \rangle = \sum_n |u_{i\mu\uparrow}^n|^2 f(E_n) + \sum_n |v_{i\mu\downarrow}^n|^2 [1 - f(E_n)]. \quad (8)$$

Here $f(x)$ is the Fermi distribution function. The LDOS is expressed by

$$\rho_i(\omega) = \sum_{n\mu} [|u_{i\mu\sigma}^n|^2 \delta(E_n - \omega) + |v_{i\mu\bar{\sigma}}^n|^2 \delta(E_n + \omega)], \quad (9)$$

where the delta function $\delta(x)$ has been approximated by $\Gamma/\pi(x^2 + \Gamma^2)$ with the quasiparticle damping $\Gamma = 0.002$.

Following Ref.17, we focus our studies on the optimal doped sample with $x = 0.56$, which is used throughout the present work. The pairing strength is chosen to be $V_{i\mu j\nu} = 0.6\text{eV}$ for all pairing states. The numerical calculation is performed on a 24×24 lattice with the periodic boundary conditions. In this paper, the energy and length are measured in units of eV and the Bi-Bi distance a respectively. To calculate the LDOS, a 80×80 supercell technique is used.

To search for the possible pairing symmetries, we consider onsite, NN and NNN singlet pairings as well as

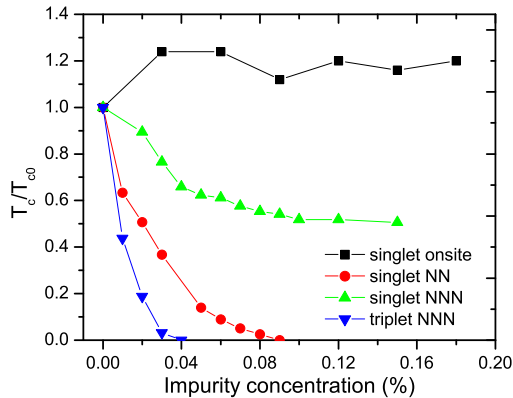


FIG. 1: (Color online) The impurity concentration dependence of the reduced critical transition temperature T_c/T_{c0} for various pairing states, where T_{c0} is the critical transition temperature without any impurity.

NNN triplet pairing. The SC order parameters are calculated self-consistently according to the BdG technique with random initial values. For the onsite singlet pairing, the calculated SC order parameter is isotropic, so it is a conventional s-wave state. For the singlet pairing between the NN sites, the calculated order parameter has amplitude $+\Delta_0$ along the x direction and $-\Delta_0$ along the y direction, resulting in the d-wave state with the k -dependent pairing form $\Delta(k) = \Delta_0(\cos k_x - \cos k_y)$. In order to study the impurity effect in the extended s-wave state with the singlet pairing between NN sites, we set the same sign along the x and y directions so that the gap function has the form $\Delta(k) = \Delta_0(\cos k_x + \cos k_y)$. For the singlet pairing between NNN sites, the order parameter has amplitude $+\Delta_1$ along the $x = y$ direction and $-\Delta_2$ along the $x = -y$ direction with $\Delta_1 \neq \Delta_2$ due to the anisotropic hopping. Hence, the gap consists of both s- and d- wave components. For the triplet pairing between NNN sites, the pairing interaction is only considered in the $x = y$ direction of the p_x orbit and in the $x = -y$ direction of the p_y orbit. The calculated amplitude of the order parameter has the form $\Delta_{i,i+x+y} = -\Delta_{i+x+y,i}$ of the p_x orbit and $\Delta_{i,i+x-y} = -\Delta_{i+x-y,i}$ of the p_y orbit, resulting in the p-wave state with k -dependent pairing form $\Delta(k) = \Delta_0 \sin(k_x \mp k_y)$, where “-,” “+” are for the two orbits respectively.

We first study the multiple-impurity effect for various pairing states. In this case, the impurities are randomly distributed in the 24×24 lattice. The zinc element has a stable d^{10} configuration in the alloy and can serve as the best non-magnetic impurity. If the Zn impurity is located in the BiS₂ layer, the scattering is quite strong. Hence, only the strong impurity potential $V_s = 10\text{eV}$ is considered here. We have considered 20 sets of multiple-impurity configurations and the critical transition temperature is the average value of these configurations. The

impurity concentration dependence of the reduced critical transition temperature T_c/T_{c0} is presented in Fig. 1, where T_{c0} is the critical transition temperature without any impurity. As seen, for the onsite pairing s-wave state, the critical temperature T_c does not decrease with the increasing impurity concentration. While, it decreases with increasing impurity concentration for the other pairing states, such as spin singlet NN pairing, NNN pairing, and spin triplet NNN pairing states. For the spin singlet NNN pairing state, the critical temperature decreases rapidly in the low impurity concentration region ($\leq 5\%$), then it almost saturates with further increasing the impurity concentration. For the spin singlet NN pairing d-wave state and the spin triplet NNN pairing p-wave state, the critical transition temperature decreases with the increasing impurity concentration monotonically. While, the reduction of the critical transition temperature in the p-wave state is faster than that in the d-wave state.

Generally, studying the non-magnetic impurity effect on superconductors helps greatly to investigate the pairing symmetry. It is well known that superconductivity is robust against small concentrations of non-magnetic impurities in conventional s-wave superconductors, according to the Anderson’s theorem³⁹. One possible explanation is that since superconductivity is due to the instability of the Fermi surface to pairing of time-reversed quasiparticle states, any perturbation that does not lift the Kramers degeneracy of these states does not affect the mean-field SC transition temperature. However, a magnetic impurity, owing to the effect of breaking the time reversal symmetry, can break Cooper pairs easily. For instance, MgB₂ is a BCS-type superconductor with the electron-phonon coupling and its symmetry is a s-wave, revealed by enormous experiments⁴⁰, such as the isotope effect by the substitution of ¹¹B⁴¹ and the observation of a coherent peak in the nuclear magnetic resonance (NMR) experiment⁴². Zn ions have a full d shell and are nominally non-magnetic. Effect of Zn-substitution on the MgB₂ superconductor shows that the critical transition temperature T_c is almost unchanged with small Zn-concentration, while T_c is significantly suppressed by the substitution of magnetic ions⁴³. These results are consistent with the Anderson’s theorem. For the BiS₂-based superconductor, the density function based calculations shows that this material may be a conventional s-wave superconductor with a large electron-phonon coupling constant^{18,19}, but the non-magnetic impurity effect in the multi-orbital system is subtle. For the iron-based superconductors, theoretical calculations have shown that, in the strong scattering limit, the non-magnetic impurity effect on the s_{\pm} -wave state is severe and similar to the effect on the d-wave SC state⁴⁴. Experimentally, it is found that with the presence of Zn impurity, the SC transition temperature increases in the under-doped regime, remains unchanged in the optimally doped regime and is severely suppressed in the over-doped regime⁴⁵. The severe suppression of T_c in the over-doped regime may be well explained within the scenario of s_{\pm} -wave symmetry.

On the other hand, the insensitivity of the impurity effect in the under-doped and optimally doped regimes is not in accordance with the s_{\pm} pairing but with the s-wave state corresponding to the same signs of the relative order parameters between the hole and electron Fermi pockets. A very recent theoretical calculation based on a two-orbital model for the iron-based superconductors also indicates that T_c is insensitive to the Zn impurity if the SC order parameter has a large s-wave component with the relatively strong onsite pairing strength⁴⁶. For the BiS₂-base superconductor, the symmetry of the order parameter is an isotropic s-wave state if considering the onsite pairing. As revealed by our numerical calculation presented in Fig. 1, T_c is not sensitive to the non-magnetic impurities in the s-wave state, which is consistent with the results in the iron-based compounds discussed above. Note that there is an enhancement of T_c by the non-magnetic impurity substitution, which is perhaps due to the enhanced density of state near the Fermi level^{47,48}.

In contrast to the isotropic s-wave superconductors, non-magnetic impurities are pairing breakers in anisotropic superconductors, such as heavy fermion superconductors⁴⁹ and cuprats⁵⁰. Based on the second Born approximation and the strong-coupling Eliashberg theory, impurity-induced T_c suppression in d-wave cuprate superconductors has been predicted⁵⁰. Experimentally, Zn substitution for Cu in the high- T_c cuprates dramatically suppresses superconductivity. For instance, it has been shown that an impurity concentration of 2-3 at.% (per Cu) reduces T_c to half or less for unsubstituted systems over a wide region of hole doping level in Zn substituted La_{2-y}Sr_yCuO₄ and YBa₂Cu₃O_{6+δ}⁵¹⁻⁵³. In our self-consistent calculation, it is found that the pairing symmetry is d-wave in the NN singlet paring state for BiS₂-compounds. The critical transition temperature T_c is suppressed significantly by small concentration of non-magnetic impurities. This result is similar to that of high T_c cuprate superconductors, indicating the pairing breaking effect in d-wave SC gap. While in the NNN singlet paring state, T_c is suppressed quickly for small impurity concentration then saturates with further increasing impurities. According to our calculation, the SC gap has both s- and d- wave components. Hence, the suppression of T_c is the consequence of the pairing break effect of the d-wave component in the SC gap, but the saturation of T_c is due to the s-wave component.

In principle, non-magnetic impurities are pair breakers for higher-orbital momentum states like p-wave state³⁰. The reduction of T_c due to non-magnetic impurity scattering in Sr₂RuO₄ compound with p-wave like symmetry has been calculated with the conventional Abrikosov-Gorkov formula²⁸, which has been proved by the substitution of non-magnetic impurity Ti⁴⁺ ions^{54,55}. For the BiS₂-based superconductors, possible spin triplet p-wave paring state is proposed^{11,17}. From our self-consistent calculation, the rapid depression of T_c by the non-magnetic impurity substitution can be tested experimentally.

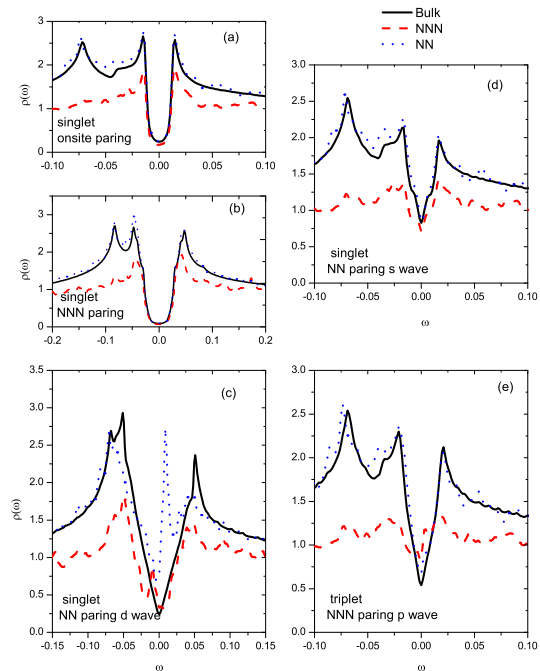


FIG. 2: (Color online) LDOS spectra around a non-magnetic impurity at various paring states. The impurity strength is set to be $V_s = 10\text{eV}$. The solid (black) curves are the LDOS spectra in the bulk, the dash dotted (green) curves are the LDOS spectra at the NN sites of the impurity, and the dashed (red) curves are the LDOS spectra at the NNN sites of the impurity. (a): Spin singlet of onsite paring state; (b): Spin singlet of NNN paring state; (c): Spin singlet of NN paring for d wave state; (d): Spin singlet of NN paring for extended s wave state; (e): Spin triplet of NNN paring for p wave state.

We now turn to study the single impurity effect in the LDOS spectra of various paring symmetries. The calculated results are presented in Fig. 2(a)-2(e). Shown in Fig. 2(a) is the LDOS spectra around a non-magnetic impurity for the isotropic s-wave paring state. As it can be seen, the LDOS spectrum in the bulk has a U-shaped bottom, indicating a full SC gap. Outside the gap, the van Hove singularity peak is clearly seen. At the NN site of the impurity, the LDOS spectrum is almost unchanged compared with that in the bulk, while at the NNN site of the impurity, the SC coherence peaks in the LDOS spectrum are depressed. From the above result, it is found that there is no impurity state in the isotropic s-wave paring state. In general, the potential scattering impurities are not pair breakers in the s-wave case according to the Anderson theorem³⁰. Presented in Fig. 1(b) is the LDOS spectra for the spin singlet NNN paring state. The results are similar to the case of the onsite paring state, i.e., the LDOS spectrum has a U-shaped bottom and no impurity state occurs inside the SC gap.

The LDOS spectra for the spin singlet NN paring d-wave state are shown in Fig. 2(c). It is found that the

LDOS spectrum has a V-shaped bottom in the bulk, indicating the nodal characteristics. At the NN site of the impurity, there is a sharp resonance peak at $\omega_0 = 9\text{meV}$ in the LDOS spectrum. At the NNN site of the impurity, there is also a weak in-gap peak at $\omega_0 = -9\text{meV}$. Note that, the SC coherence peaks are also depressed obviously by the impurity at the NNN site. The resonance peak inside the SC gap at the NN site of the impurity is a general feature in a d-wave superconductor, which has already been reported in cuprate superconductors both theoretically³⁰ and experimentally⁵⁶. The LDOS spectra for the spin singlet NN paring s-wave state are presented in the Fig. 2(d). The LDOS spectrum in the bulk still has a V-shaped bottom. The LDOS spectrum at the NN site of the impurity is almost unchanged compared with that in the bulk. Similar to the spin singlet onsite and NNN paring states, there is no impurity state in this case. However, at the NNN site of the impurity, the SC coherence peaks are almost flattened, which is quite different from those in the previous cases.

The LDOS spectra for the spin triplet NNN paring p-wave state are shown in Fig. 2(e). As one can see, the LDOS spectrum in the bulk is also V-shaped with nodal characteristics. Previously, a fully nodeless SC gap was found in the Sr_2RuO_4 superconductors from the scanning tunnelling microscopy experiments⁵⁷, which is quite different from our result. This is most due to its complex paring symmetry without nodes at the Fermi surface, i.e., $\sin p_x + i\sin p_y$ wave or $\sin(p_x + p_y) + i\sin(-p_x + p_y)$ wave⁵⁸. At the NN site of the impurity, there is a small in-gap peak at $\omega_0 = 3\text{meV}$ in the spectrum. At the NNN site of the impurity, two in-gap peaks are found at $\omega_0 = \pm 3\text{meV}$, where the in-gap peak at the positive energy is much stronger than that at the negative energy. Moreover, the SC coherence peaks are almost flattened by the impurity, similar to that of the spin singlet NN paring s-wave state. From the above discussion, one can conclude that there are impurity resonance peaks only in the spin singlet NN paring d-wave state. The resonance peak is very sharp in the LDOS spectrum at the NN site. However, two in-gap peaks occur in the spectrum at the NNN site for the p-wave paring state and the SC coherence peaks are almost flattened by the impurity. These results can be used to detect the paring symmetry in the BiS_2 -based superconductors.

The potential strength response of the impurity state is also calculated. The impurity states at various potential strengths for the d-wave paring state are presented in Fig. 3(a)-3(e). As seen in Fig. 3(a)-3(b), for the positive impurity potential the resonance peak at the NN site of the impurity decreases with the decreasing of the potential strength. At the impurity potential $V_s = 1\text{eV}$, the resonance peak almost disappears and merges into the SC coherence peak. However, the situation is quite different in the case of the negative impurity potential. At the strong impurity potential $V_s = -10\text{eV}$, there is also a sharp resonance peak at the NN site of the impurity located at $\omega_0 = 6\text{meV}$, which is shifted to the lower energy

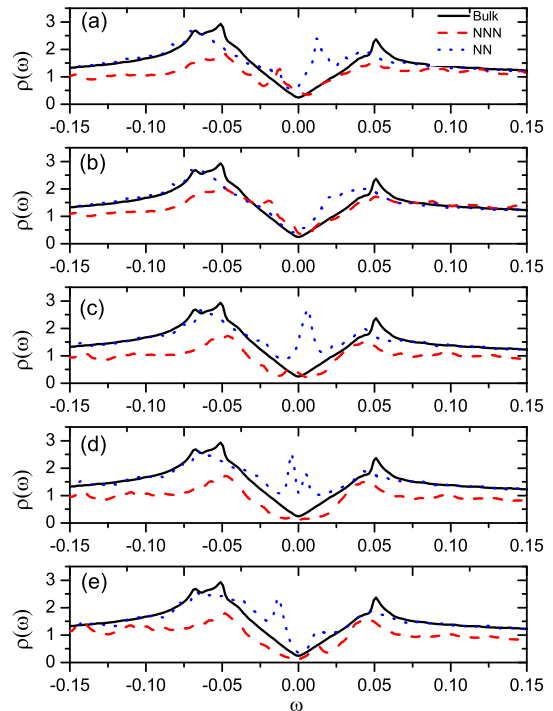


FIG. 3: (Color online) LDOS spectra around a non-magnetic impurity at various potential strengths for d-wave paring state. (a): $V_s = 3\text{eV}$; (b): $V_s = 1\text{eV}$; (c): $V_s = -10\text{eV}$; (d): $V_s = -2\text{eV}$; (e): $V_s = -1\text{eV}$.

compared with that of the impurity potential $V_s = 10\text{eV}$. With the impurity potential decreasing, as shown in Fig. 3(d), the resonance peak at the NN site of the impurity splits into two peaks located at $\omega_0 = \pm 4.5\text{meV}$, and the peak at the negative energy is much stronger than that at the positive energy. With the impurity potential $V_s = -1\text{eV}$, there are also two in-gap peaks at the NN site of the impurity located at $\omega_0 = \pm 13.5\text{meV}$, and the peak at the positive energy almost disappears.

The potential strength response of the impurity states for the p-wave paring state is presented in Fig. 4(a)-4(c). For the positive impurity strength, the LDOS spectra are similar to that of $V_s = 10\text{eV}$, i.e., two in-gap peaks occurring at the NNN site of the impurity. These results are not presented for simplicity. Here, we focus on the LDOS spectra of the negative impurity potential for the p-wave paring state. As it can be seen, at the NN site of the impurity, the LDOS spectra are almost featureless compared with those in the bulk. However, there is an in-gap peak in the LDOS spectra at the NNN site of the impurity, and the SC coherence peaks are almost flattened. Moreover, the location of the in-gap peak shifts from $\omega_0 = 1.5\text{meV}$ at $V_s = -10\text{eV}$ to $\omega_0 = -4.5\text{meV}$ at $V_s = -1.5\text{eV}$.

In summary, the impurity effects are studied for the BiS_2 -layered superconductors based on a two-orbital

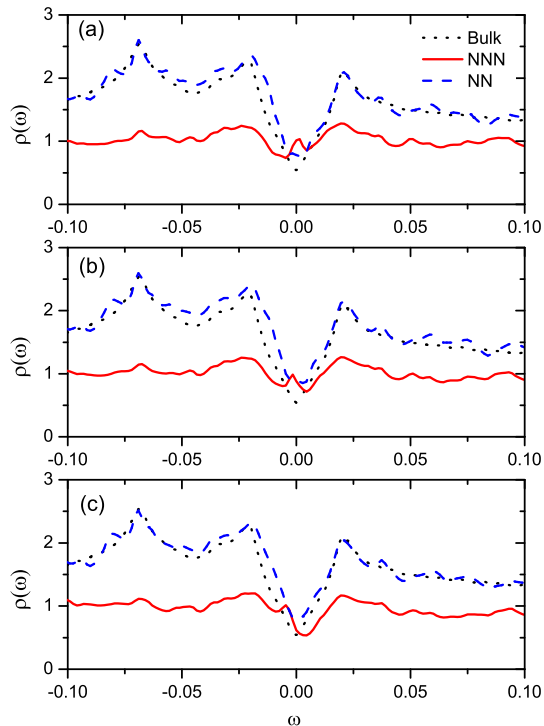


FIG. 4: (Color online) LDOS spectra around a non-magnetic impurity at various potential strengths for p-wave paring state. (a): $V_s = -10\text{eV}$; (b): $V_s = -3\text{eV}$; (c): $V_s = -1.5\text{eV}$.

model with the BdG technique. From the calculation of multiple-impurity effect, the significant reduction of T_c is found for the spin singlet NN paring d-wave state and the spin triplet NNN paring p-wave state, while no depression of T_c for isotropic s-wave state. The single-impurity effects for various paring states are also calculated. The impurity resonance peak in the LDOS spectrum is found only for the d-wave state. For the spin triplet NNN paring p-wave state, two in-gap peaks occur in the case of positive impurity potential, while a single in-gap peak is found for the negative impurity potential, and it shifts towards the lower energy with the decreasing of the potential strength. These results can be used to detect the paring symmetry of the BiS_2 -based superconductors.

This work is supported by the research foundation of the Nanjing university of posts and telecommunications (NY211146). We also appreciate the mathematical laboratory of the college of science, Nanjing university of posts and telecommunications for the technical support.

-
- ¹ W. E. Pickett, *Rev. Mod. Phys.* **61**, 433 (1989).
² Y. Maeno et al., *Nature* **372**, 532 (1994).
³ J. Nagamitsu, N. Nakagawa, T. Muranaka, Y. Zenitani, and J. Akimitsu, *Nature* **410**, 63 (2001).
⁴ K. Takada et al., *Nature* **422**, 53 (2003).
⁵ Y. Kamihara et al., *J. Am. Chem. Soc.* **130**, 3296 (2008).
⁶ Yoshikazu Mizuguchi, Hiroshi Fujihisa, Yoshito Gotoh, Katsuhiro Suzuki, Hidetomo Usui, Kazuhiko Kuroki, Satoshi Demura, Yoshihiko Takano, Hiroki Izawa and Osuke Miura, *Phys. Rev. B* **86**, 220510(R) (2012).
⁷ Yoshikazu Mizuguchi, Satoshi Demura, Keita Deguchi, Yoshihiko Takano, Hiroshi Fujihisa, Yoshito Gotoh, Hiroki Izawa and Osuke Miura, *J. Phys. Soc. Jap.* **81** (2012) 114725.
⁸ Satoshi Demura, Yoshikazu Mizuguchi, Keita Deguchi, Hiroyuki Okazaki, Hiroshi Hara, Tohru Watanabe, Saleem James Denholme, Masaya Fujioka, Toshinori Ozaki, Hiroshi Fujihisa, Yoshito Gotoh, Osuke Miura, Takahide Yamaguchi, Hiroyuki Takeya, and Yoshihiko Takano, arXiv:1207.5248.
⁹ Jie Xing, Sheng Li, Xiaping Ding, Huang Yang and Hai-Hu Wen, *Phys. Rev. B* **86**, 214518 (2012).
¹⁰ Rajveer Jha, Shiva Kumar Singh, and V.P.S. Awana, arXiv:1208.5873.
¹¹ Hidetomo Usui, Katsuhiro Suzuki, and Kazuhiko Kuroki, arXiv:1207.3888.
¹² Sheng Li, Huan Yang, Jian Tao, Xiabin Ding, and Hai-Hu Wen, arXiv:1207.4955.
¹³ S. G. Tan, L. J. Li, Y. Liu, P. Tong, B. C. Zhao, W. J. Lu, Y. P. Sun, *Physica C*, **483**, 94 (2012).
¹⁴ Shiva Kumar Singh, Anuj Kumar, Bhasker Gahtori, Shruti, G. Sharma, S. Patnaik and V.P.S. Awana, *J. Am. Chem. Soc.* **134**, 16504 (2012).
¹⁵ V.P.S. Awana, Anuj Kumar, Rajveer Jha, Shiva Kumar, Jagdish Kumar, and Anand Pal, arXiv:1207.6845.
¹⁶ Hisashi Kotegawa, Yusuke Tomita, Hideki Tou, Hiroki Izawa, Yoshikazu Mizuguchi, Osuke Miura, Satoshi Demura, Keita Deguchi, and Yoshihiko Takano, *J. Phys. Soc. Jpn.* **81** (2012) 103702.
¹⁷ Tao Zhou and Z. D. Wang, *Journal of Superconductivity and Novel Magnetism*, DOI: 10.1007/s10948-012-2073-4 (2012).
¹⁸ Xiangang Wan, Hang-Chen Ding, Sergey Y. Savrasov and Chun-Gang Duan, arXiv:1208.1807.
¹⁹ B. Li and Z. W. Xing, arXiv:1210.1743.
²⁰ Hiroshi Takatsu, Yoshikazu Mizuguchi, Hiroki Izawa, Osuke Miura, and Hiroaki Kadowaki, *J. Phys. Soc. Jpn.* **81** (2012) 125002.
²¹ Clastin I. Sathish and Kazunari Yamaura, arXiv:1208.2818.
²² Rajveer Jha, Anuj Kumar, Shiva Kumar Singh and V.P.S. Awana, arXiv:1208.3077.
²³ Hechang Lei, Kefeng Wang, Milinda Abeykoon, Emil S. Bozin, and C. Petrovic, arXiv:1208.3189.

- ²⁴ S. G. Tan, P. Tong, Y. Liu, W. J. Lu, L. J. Li, B. C. Zhao, Y. P. Sun, arXiv:1208.5307.
- ²⁵ K. Deguchi, Y. Mizuguchi, S. Demura, H. Hara, T. Watanabe, S. J. Denholme, M. Fujioka, H. Okazaki, T. Ozaki, H. Takeya, T. Yamaguchi, O. Miura, and Y. Takano, arXiv:1209.3846.
- ²⁶ Yi Liang, Xianxin Wu, Wei-Feng Tsai, and Jiangping Hu, arXiv:1211.5435.
- ²⁷ G. B. Martins, A. Moreo, and E. Dagotto, arXiv:1212.0210.
- ²⁸ K. Miyake and O. Narikiyo, Phys. Rev. Lett. **83**, 1423 (1999).
- ²⁹ M. A. Woolf, and F. Reif, Phys. Rev. **137**, A557 (1965).
- ³⁰ A. V. Balatsky, I. Vekhter and Jian-Xin Zhu, Rev. Mod. Phys. **78**, 373 (2006).
- ³¹ Degang Zhang, Phys. Rev. Lett. **103**, 186402 (2009); Phys. Rev. Lett. **104**, 089702 (2010).
- ³² Tao Zhou, Huaixiang Huang, Yi Gao, Jian-Xin Zhu, and C. S. Ting, Phys. Rev. B **83**, 214502 (2011).
- ³³ Tao Zhou, Z. D. Wang, Yi Gao, and C. S. Ting, Phys. Rev. B **84**, 174524 (2011).
- ³⁴ Hong-Min Jiang, Jia Guo, and Jian-Xin Li, Phys. Rev. B **84**, 014533 (2011).
- ³⁵ Y. Bang, H. Y. Choi, and H. Won, Phys. Rev. B **79**, 054529 (2009).
- ³⁶ A. B. Vorontsov, M. G. Vavilov, and A. V. Chubukov, Phys. Rev. B **79**, R140507 (2009).
- ³⁷ S. L. Liu and Tao Zhou, J. Phys.: Condens. Matter **24**, 225701 (2012).
- ³⁸ Wei-Feng Tsai, Yan-Yang Zhang, Chen Fang, and Jiangping Hu, Phys. Rev. B **80**, 064513 (2009).
- ³⁹ Anderson, P. W., Phys. Rev. Lett. **3**, 325 (1959).
- ⁴⁰ Takahiro Muranaka and Jun Akimitsu, zcri **226**, 385 (2011).
- ⁴¹ S. L. Bud'ko, G. Lapertot, C. Petrovic, C. E. Cunningham, N. Anderson, and P. C. Canfield, Phys. Rev. Lett. **86**, 1877 (2001).
- ⁴² H. Kotegawa, K. Ishida, Y. Kitaoka, T. Muranaka, and J. Akimitsu, Phys. Rev. Lett. **87**, 127001 (2001).
- ⁴³ S. Xu, Y. Moritomo, K. Kato, and A. Nakamura, J. Phys. Soc. Jpn **70**, 1889 (2001).
- ⁴⁴ Bang Y, Choi H and Won H, Phys. Rev. B **79**, 054529 (2009).
- ⁴⁵ Yuke Li, Jun Tong, Qian Tao, Chunmu Feng, Guanghan Cao, Weiqiang Chen, Fu-chun Zhang and Zhu-an Xu, New Journal of Physics **12** (2010) 083008.
- ⁴⁶ Zi-Jian Yao, Wei-Qiang Chen, Yu-ke Li, Guang-han Cao, Hong-Min Jiang, Qian-En Wang, Zhu-an Xu, Fu-Chun Zhang, arXiv:1209.0709.
- ⁴⁷ A. Garg, M. Randeria and N. Trivedi, Nature Physcis **4**, 762 (2008).
- ⁴⁸ A. F. Kemper, D. G. S. P. Doluweera, T. A. Maier, M. Jarrell, P. J. Hirschfeld, and H-P. Cheng, Phys. Rev. B **79**, 104502 (2009).
- ⁴⁹ A. J. Millis, S. Sachdev and C. M. Varma, Phys. Rev. B **37**, 4975 (1988).
- ⁵⁰ R. J. Radtke, K. Levin, H.-B. Schüttler and M. R. Norman, Phys. Rev. B **48**, 653 (1993).
- ⁵¹ Gang Xiao, Marta Z. Cieplak, J. Q. Xiao and C. L. Chien Phys. Rev. B **42**, 8752 (1990).
- ⁵² P. Mendels, H. Alloul, E. J. Ansaldo, G. Collin, J.F. Marucco, C. Niedermayer, D. R. Noakes and C. E. Stronach, Phys. Rev. B **49**, 10035 (1994).
- ⁵³ Y. Fukuzumi, K. Mizuhashi, K. Takenaka, and S. Uchida, Phys. Rev. Lett. **76**, 684 (1996).
- ⁵⁴ Naoki Kikugawa and Yoshiteru Maeno, Phys. Rev. Lett. **89**, 117001, (2002); Naoki Kikugawa, Andrew Peter Mackenzie and Yoshiteru Maeno, J. Phys. Soc. Jpn **72**, 237 (2003).
- ⁵⁵ M. Minakata and Y. Maeno, Phys. Rev. B **63**, 180504(R)(2001).
- ⁵⁶ Pan, S. H., E. W. Hudson, K. M. Lang, H. Eisaki, S. Uchida, and J. C. Davis, Nature (London) **403**, 746 (2000).
- ⁵⁷ H. Suderow, V. Crespo, I. Guillamon, S. Vieira, F. Servant, P. Lejay, J.P. Brison, and J. Flouquet, New J. Phys. **11**, 093004 (2009).
- ⁵⁸ Mitsuaki Takigawa, Masanori Ichioka, Kazuhiko Kuroki, Yukio Tanaka, Phys. Rev. B **72**, 224501 (2005).